Progress In Electromagnetics Research, Vol. 133, 137–157, 2013

A POLE AND AMC POINT MATCHING METHOD FOR THE SYNTHESIS OF HSF-UC-EBG STRUCTURE WITH SIMULTANEOUS AMC AND EBG PROPERTIES

L. Zhao, D. Yang, H. Tian, Y. Ji*, and K. Xu

The State Key Laboratory of Information Photonics and Optical Communications, School of Information and Communication Engineering, Beijing University of Posts and Telecommunications, Beijing 100876, China

Abstract—The relationship between the reflection phase curve and the dispersion curve of a H-shaped slot fractal uniplanar compact electromagnetic bandgap (HSF-UC-EBG) structure is investigated in this paper. It is demonstrated numerically and theoretically that the pole (located at phi = 180 degrees) of the reflection phase curve is related to the EBG location of the dispersion curve. More specifically, the pole is always located in the bandgap and the frequency shift characteristics of the pole and the EBG location are the same. Therefore, locations of the artificial magnetic conductor (AMC) and EBG can match with the AMC point and the pole, respectively. By realizing and making appropriate use of this, we can tailor the AMC and EBG locations to coincide in the frequency region only by reducing the spectral distance (d) between the AMC point and the pole. This method can improve the computational efficiency significantly. Parametric studies have been performed to obtain guidelines for reducing d. Finally, an example to design HSF-UC-EBG structure with simultaneous AMC and EBG properties by using this technique is presented with detail steps.

1. INTRODUCTION

In the past few decades, the tremendous potential of electromagnetic bandgap (EBG) structures as circuit elements in antennas [1–9], filters [10–12], circuits [13–16] and waveguides [17] have made them a great attraction in microwave engineering community. EBG structure

Received 24 June 2012, Accepted 28 September 2012, Scheduled 18 October 2012

* Corresponding author: Yuefeng Ji (jyf@bupt.edu.cn).

can be made of dielectric only or of metallic elements printed on a metal backed dielectric material. It possesses two unique properties: artificial magnetic conductor (AMC) property and EBG property. AMC property refers to EBG structures can reflect normally incident electromagnetic wave with a zero phase shift at a frequency called "AMC point", and is commonly characterized by the reflection phase curve. EBG property refers to EBG structure can stop electromagnetic surface waves (SW) propagating in a certain frequency range called "bandgap", and is commonly characterized by the dispersion curve.

The mushroom-like EBG structure reported in [18] possess the advantage that its AMC property and EBG property are at the same frequency region due to the presence of the grounding vias. But the vias complicate the fabrication of EBG structure, particularly at upper microwave and millimeter wave frequencies. In order to simplify the fabrication, research efforts have been lead to the realization of uniplanar compact EBG (UC-EBG) structures that without vias [14]. However, in absence of ground vias, the AMC property and EBG property do not normally coincide in the frequency domain. In order to design UC-EBG structures with simultaneous AMC and EBG properties, some related studies were published in [19–21]. These research investigated the reflection phase curve and dispersion curve simultaneously. It is known that there is a substantial difference between the analysis of reflection phase curve and dispersion curve. The analysis of dispersion curve is complex and extremely time-consuming, while the analysis of the reflection phase curve is simple and extremely efficient.

In this paper, we present a pole and AMC point match method based only on analyzing the reflection phase curve, by revealing the relationship between the reflection phase curve and dispersion curve of a HSF-UC-EBG structure (Figure 1). It is revealed that the pole (hollow O-rings in the reflection phase curve in Figure 2(b)) is located in the frequency range of bandgap (light gray area in Figure 4). Moreover, the pole and the bandgap have same frequency shift characteristics. Therefore, tailoring the AMC and EBG properties to coincide in the frequency region can be simplified to reduce the spectral distance (d) between the "AMC point" (solid dots in Figure 2(b)) and the pole.

The contents of this paper are organized as follows: Section 2 describes the design of the HSF-UC-EBG structure and presents the relationship between its reflection phase curve and dispersion curve on the basis of full-wave analysis and theoretical analysis. Parametric studies on reducing the spectral distance (d) of the "AMC point" and pole is preformed in Section 3. Some tailoring guidelines and an

example to design HSF-UC-EBG structure with simultaneous AMC and EBG properties by following the pole and AMC point matching method are presented in Section 4. Finally, some conclusions are made in Section 5.

2. DESIGN OF HSF-UC-EBG STRUCTURE AND ITS PROPERTY

2.1. Geometry of the HSF-UC-EBG Structure

We use the two-dimensional H-shaped fractal unit cell of photonic crystal [22] to construct an anisotropic HSF-UC-EBG structure since anisotropic EBG structures possess rather general dispersion properties to furbish a complete illustrative example. It consists of a patch with period array of H-shaped fractal slots printed on a metal backed substrate (Figure 1(a)). The thickness and the permittivity of substrate are denoted by h and ε_r, respectively. Figure 1(b) shows the geometry of the unit cell. The unit cell size, also the period of the HSF-UC-EBG structure is denoted by P. The fractal shape begins as a simple H-shaped slot with length L and width W, respectively. There are four second-level H-shaped slots whose length and width are $L/2$ and W, respectively, around the first-level H-shaped slot. Figure 1(c) shows the first Brillouin zone (BZ) and the irreducible Brillouin zone (IBZ) of the HSF-UC-EBG structure.

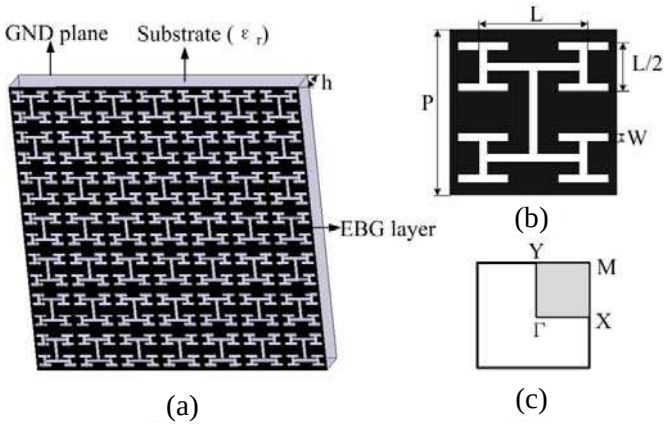

Figure 1. (a) Geometry of the HSF-UC-EBG structure. (b) Unit cell of the HSF-UC-EBG structure. (c) The first Brillouin zone (BZ) of the HSF-UC-EBG structure, where the shaded part is the irreducible Brillouin zone (IBZ).

2.2. Relationship between the Reflection Phase and Dispersion Curve Based on Full-wave Analysis

In this section, the AMC and EBG properties of the HSF-UC-EBG structure are investigated based on the High Frequency Structure Simulator (HFSS). The infinite periodic HSF-UC-EBG structure is simulated through modeling one unit cell and applying the periodic boundary conditions (PBC).

2.2.1. Identification of the Poles of the Reflection Phase Curve

Figure 2(a) shows the modeling setup for the reflection phase simulation of the HSF-UC-EBG structure. The master/slave boundary condition is assigned as the PBC to each pair of the opposite side walls of the model, which means this unite cell belongs to an infinitely array of HSF-UC-EBG structure. A Floquet port is placed about 6 times the height (h) of the substrate above the HSF-UC-EBG structure and de-embedded on the HSF-UC-EBG surface. Figure 2(b) shows the reflection phase curve of a normally incident plane wave when the parameters of HSF-UC-EBG structure are $h = 0.8\,\text{mm}$, $\varepsilon_r = 10.2$, $P = 6\,\text{mm}$, $L = 3.6\,\text{mm}$, $W = 0.3\,\text{mm}$. As can be seen, there are two kinds of special points in the reflection phase curve, and we identify them to AMC points and poles, respectively. AMC

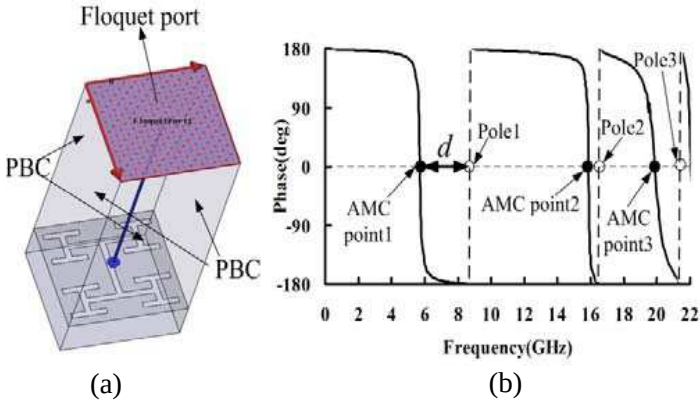

Figure 2. (a) Simulation model for determining the reflection properties of the HSF-UC-EBG structure. (b) Reflection phase curve of the HSF-UC-EBG structure with parameters of $h = 0.8\,\text{mm}$, $\varepsilon_r = 10.2$, $P = 6\,\text{mm}$, $L = 3.6\,\text{mm}$, $W = 0.3\,\text{mm}$. AMC points (marked by solid dots) and poles (marked by hollow O-rings) are appearing in pairs.

points are those frequencies where the reflection phases are zeros. Poles are those frequencies where the reflection phases curve exhibits abrupt discontinuities between $-180°$ and $180°$. In order to describe conveniently, some hollow O-rings are introduced in the center of the abrupt discontinuities to identify the poles. As can be seen from Figure 2(b) the AMC points and poles appear in pairs.

2.2.2. Relationship between the Pole and the Dispersion Curve

It is know that the higher frequency modes above the substrate cone of the dispersion curve are leaky modes, only the lower frequency modes are investigated in this paper, which means only the first AMC point, first pole and first bandgap are investigated in this paper.

To study the relationship between the pole and dispersion curve, the HSF-UC-EBG structure with different substrate thickness h = 0.4 mm, 0.6 mm, 0.8 mm, and 1.0 mm are studied, respectively. The other parameters are kept the same as those in Figure 2 in the above four cases. Figure 3 and Figure 4 show the reflection phase curve and dispersion curve of the HSF-UC-EBG structure with varying substrate thickness from 0.4 mm to 1.0 mm, respectively. It is observed from Figure 3 and Figures 4(a)–(d) that the four poles (8.23 GHz, 8.53 GHz, 8.73 GHz and 8.83 GHz) are located in the frequency range of the four bandgaps (6.66–9.41 GHz, 6.83–9.41 GHz, 7.00–9.54 GHz and 7.16–9.56 GHz), respectively. Moreover, the frequency shift characteristic of the EBG location follows the moving trend of the pole: both of them shift to higher frequency as the substrate thickness is increased.

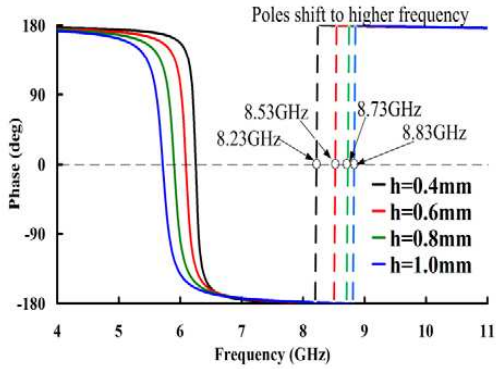

Figure 3. Reflection phase curve of the HSF-UC-EBG structure with substrate thickness (h) varying from 0.4 mm to 1.0 mm. The other parameters are kept the same as those in Figure 2. The poles shift to higher frequency as substrate thickness increases.

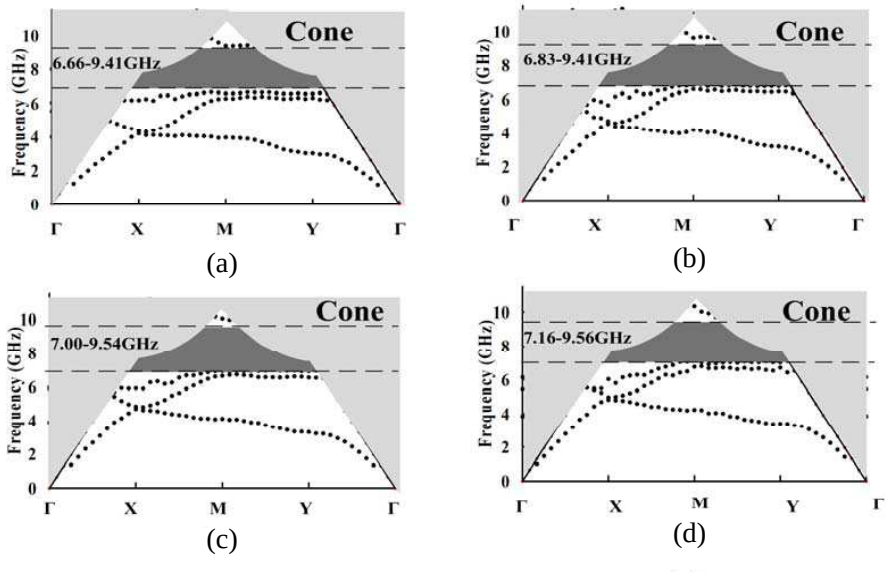

Figure 4. Dispersion curve of the HSF-UC-EBG structure with (a) $h = 0.4\,\text{mm}$, (b) $h = 0.6\,\text{mm}$, (c) $h = 0.8\,\text{mm}$, (d) $h = 1.0\,\text{mm}$ and the other parameters are kept the same as those in Figure 2. The EBG location shift to higher frequency as substrate thickness increases.

2.3. Theoretical Analysis

UC-EBG structures are essentially periodic frequency selective surfaces (FSS) [23–25] printed on ground backed dielectric slabs. They can be analyzed by the equivalent LC-network associated with the FSS. The analytical expression of the equivalent admittance Y_{FSS} (k, ω) of the network is given by [26]:

$$Y_{FSS}(k,\omega) = \frac{j\omega C_0\left(\omega^2 - [\omega_{Z_1}(k)]^2\right)\left(\omega^2 - [\omega_{Z_2}(k)]^2\right)\ldots\left(\omega^2 - [\omega_{Z_n}(k)]^2\right)}{\left(\omega^2 - [\omega_{P_1}(k)]^2\right)\left(\omega^2 - [\omega_{P_2}(k)]^2\right)\ldots\left(\omega^2 - [\omega_{p_n}(k)]^2\right)}$$
$$= jY = |Y|\, e^{j\phi_y} \tag{1}$$

where

$$\omega_{p_1}(k) < \omega_{z_1}(k) < \omega_{p_2}(k) < \omega_{z_2}(k) < \ldots < \omega_{p_n}(k) < \omega_{z_n}(k) \tag{2}$$

C_0 is a constant independent on ω and k the wavenumber. ω_{z_n} and ω_{P_n} are the nth zero and pole, respectively.

The impendence $Z_{FSS}(k,\omega)$ of the network is the reciprocal of Y_{FSS} (k, ω), and is given by:

$$Z_{FSS}(k,\omega) = \frac{1}{Y_{FSS}(k,\omega)} = \frac{e^{-j\phi_y}}{|Y|} = \frac{e^{j\phi_x}}{|Y|} \tag{3}$$

From Equations (1) and (3), and equation (2), two conclusions can be easily deduced,

i) If $\omega_{z_{(n-1)}} < \omega < \omega_{p_n}, Y > 0, \phi_y > 0,$ hence, $\phi_x = -\phi_y < 0.$

ii) If $\omega_{p_n} < \omega < \omega_{z_n}, Y < 0, \phi_y < 0,$ hence, $\phi_x = -\phi_y > 0.$

From i) and ii), we can see that the phase is negative when the frequency is lower than the pole, while it is positive when the frequency is higher than the pole. Therefore, it is easy to see that the phase curve of the Z_{FSS} (k, ω) exhibits an abrupt discontinuity at the pole. According to the equivalent circuit model, the phase of the reflection coefficient is related to Z_{FSS} (k, ω), therefore, there will also be an abrupt discontinuity in the reflection phase curve in corresponding to the pole, as can be seen from Figure 2(b).

In addition, the pole is related to the SW bandgap and the frequency shift characteristic of the EBG location can be identified by the moving trend of the pole, according to [23]. The numerical simulations and the theoretical analysis are in good agreement in predicting the relationship between the pole and SW bandgap.

From the above studies, we can see that the AMC location and EBG location are related to the AMC point and pole, respectively. Based on this, we obtain a new method to tailoring the AMC and EBG properties to coincide in the frequency region, which is reducing the spectral distance (d) between the AMC point and the pole. Therefore, unlike other methods reported by others, parametric studies only need to be performed on the reflection phase curve, which is very valuable from the computational efficiency viewpoint.

3. PARAMETRIC STUDIES ON REDUCING *d*

It has been revealed that the AMC and EBG properties can be tailoring to coincide in the frequency region by reducing the spectral distance (d) between the AMC point and the pole. In this section, parametric studies are performed to obtain guidelines on reducing d. The reflection phase curve of the HSF-UC-EBG structure is mainly determined by these five parameters: substrate thickness (h), substrate permittivity (ε_r), unit cell size (P), slot length (L), and slot width (W).

According to [18], as long as the wavelength is much longer than the size of the individual cells, the surface impendence can be

represented by an equivalent parallel resonant L-C circuit. For the HSF-UC-EBGs, the total equivalent inductance L_t is mainly sheet inductance L_s, while the total equivalent capacitance C_t is mainly composed of sheet capacitance C_s and gap capacitance C_g. According to [27, 28], the equivalent parameters of the HSF-UC-EBGs can be approximated by the following given relations:

$$L_t \approx L_s = \mu_0 \times h \tag{4}$$

$$C_t \approx C_S + C_g \tag{5}$$

where,

$$C_S = \varepsilon_0 \times \varepsilon_r \times \frac{P^2}{h} \tag{6}$$

$$C_g = \frac{k \times L \times (\varepsilon_0 + \varepsilon_r)}{\pi} \times \operatorname{arcosh}\left(\frac{P}{W}\right) \tag{7}$$

where, k is a positive constant. From Equations (4) to (7), we can see that the substrate thickness h contributing to the change in both capacitance and inductance, while permittivity ε_r, unit cell size P, slot length L and slot width W contributing to the change in capacitance only.

3.1. Substrate Thickness (h) Effect

The substrate thickness (h) plays an important role in determining the reflection phases. To study the effect of substrate thickness, the other

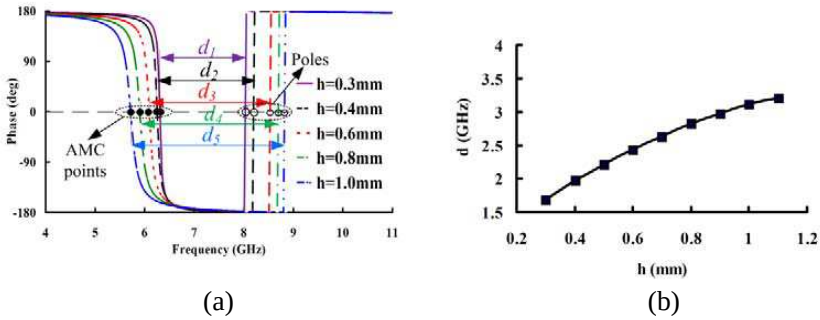

(a) (b)

Figure 5. (a) Reflection phase curve with substrate thickness h = 0.3 mm (violet), h = 0.4 mm (black), 0.6 mm (red), 0.8 mm (green), 1.0 mm (blue). (b) Spectral distance (d) between AMC point and pole versus h. The other parameters are kept the same as those in Figure 2. As h decreases, d increases.

parameters of the HSF-UC-EBG structure are kept the same as those in Figure 2. Substrate thickness changes from 0.4 mm to 1.0 mm.

Figure 5(a) shows the reflection phase curve of the HSF-UC-EBG structure with different substrate thickness (h). Figure 5(b) presents the spectral distance (d) versus the substrate thickness (h), and Table 1 lists the data of the AMC point, the pole and the spectral distance (d) between them when substrate thickness (h) varies. It is observed that when the substrate thickness is decreased, the spectral distance decreases.

For example, when the substrate thickness is $h = 1.1$ mm, the spectral distance is $d = 3.21$ GHz; when the substrate thickness is decreased to $h = 0.3$ mm, the spectral distance decreases to $d =$

Table 1. Substrate thickness effect.

h (mm)	AMC point (GHz)	Pole (GHz)	d (GHz)
0.3	6.29	7.97	1.68
0.4	6.25	8.23	1.98
0.5	6.17	8.38	2.21
0.6	6.09	8.53	2.44
0.7	6.00	8.63	2.63
0.8	5.90	8.73	2.83
0.9	5.81	8.78	2.97
1.0	5.71	8.83	3.12
1.1	5.66	8.87	3.21

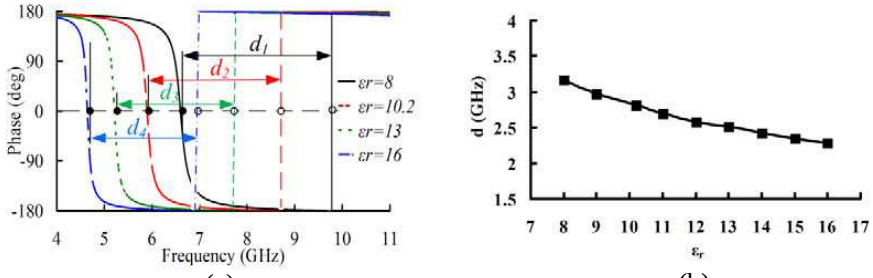

Figure 6. (a) Reflection phase curve with substrate permittivity $\varepsilon_r = 8$ (black), 10.2 (red), 13 (green), 16 (blue). (b) Spectral distance (d) between AMC point and pole versus ε_r. The other parameters are kept the same as those in Figure 2. As ε_r decreases, d increases.

1.68 GHz. This is because that as the substrate thickness is decreased; the AMC point goes up, while the pole drops. Thus, thinner substrate thickness would be chosen in order to reduce d.

3.2. Substrate Permittivity (ε_r) Effect

Relative permittivity (ε_r), also called the dielectric constant, is an effective parameter used to control the spectral distance. The HSF-UC-EBG structure analyzed here has the same parameters as those shown in Figure 2, except that permittivity is changed from 8 to 16. The reflection phase curve and the spectral distance versus permittivity are plotted in Figures 6(a) and (b), respectively. The detailed data are listed in Table 2. It is observed that if ε_r is increased, d will reduce. For instance, the spectral distance is $d = 3.17$ GHz for the case of $\varepsilon_r = 8$, while it reduces to $d = 2.28$ GHz for the case of $\varepsilon_r = 16$. It is also observed that both the AMC point and the pole shift to lower frequency as ε_r increases, because when ε_r is increased, the equivalent capacity C_t is increased.

3.3. Unit Cell Size (P) Effect

The unit cell size of UC-EBG structures can be scaled. In order to study the effect of the unit cell size, a scale factor (SF) is introduced in this paper. During this investigation, SF varies from 1 to 1.8, which means the unit cell size changes from 6 mm to 10.8 mm. Other parameters of the HSF-UC-EBG structure are kept the same as those in Figure 2.

Table 2. Substrate permittivity effect.

ε_r	AMC point (GHz)	Pole (GHz)	d (GHz)
8	6.60	9.77	3.17
9	6.25	9.22	2.97
10.2	5.90	8.72	2.82
11	5.68	8.38	2.70
12	5.45	8.03	2.58
13	5.21	7.72	2.51
14	4.99	7.42	2.43
15	4.78	7.12	2.34
16	4.64	6.92	2.28

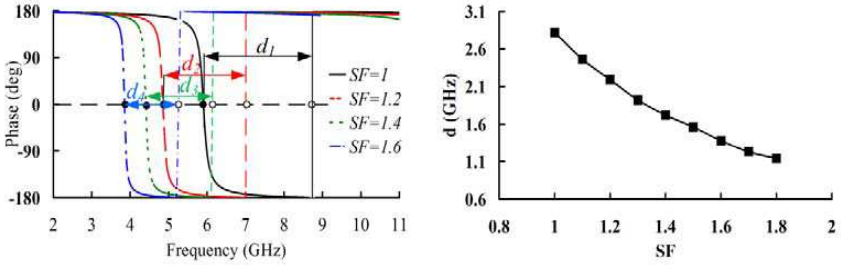

Figure 7. (a) Reflection phase curve with scale factor (SF) of the unit cell size SF = 1 (black), 1.2 (red), 1.4 (green), 1.6 (blue). (b) Spectral distance (d) between AMC point and pole versus SF. The other parameters are kept the same as those in Figure 2. As SF increases, d decreases.

Table 3. Unit cell size effect.

SF (mm)	AMC point (GHz)	Pole (GHz)	d (GHz)
1	5.90	8.72	2.82
1.1	5.32	7.78	2.46
1.2	4.84	7.03	2.19
1.3	4.60	6.52	1.92
1.4	4.41	6.13	1.72
1.5	4.11	5.67	1.56
1.6	3.85	5.23	1.38
1.7	3.64	4.87	1.23
1.8	3.44	4.58	1.14

The reflection phase curve and the spectral distance versus scale factor (SF) are plotted in Figures 7(a) and (b), respectively. The detailed data are listed in Table 3. It is observed that if the scale factor increased, the spectral distance would be decreased. For instance, the spectral distance is $d = 2.82$ GHz for the case of SF = 1, while it is $d = 1.14$ GHz for the case of SF = 1.8. In addition, AMC point and pole shift to lower frequency as the scale factor is increased; this is due to that the operating wavelength of EBG structures is proportional to its unit cell size.

3.4. Slot Length (L) Effect

According to the LC model, the slots introduce a gap capacitance C_g for the equivalent LC circuits. The value of C_g is proportional to the length (L) of the slot according to Equation (6).

Therefore, the value of L should be chosen in a certain range for the following two reasons: first, it cannot be too big since the unit cell size is fixed. Second, it cannot be too small, or there would be insufficient capacitance to form a bandgap. During this investigation, the slot length is increased from 3.0 mm to 3.8 mm and the other parameters are kept the same as those in Figure 2.

Table 4. Slot length effect.

L (mm)	AMC point (GHz)	Pole (GHz)	d (GHz)
3.0	6.79	10.68	3.89
3.1	6.58	10.23	3.65
3.2	6.45	9.93	3.48
3.3	6.28	9.58	3.30
3.4	6.15	9.27	3.12
3.5	6.00	8.97	2.97
3.6	5.88	8.73	2.85
3.7	5.80	8.48	2.68
3.8	5.68	8.28	2.60

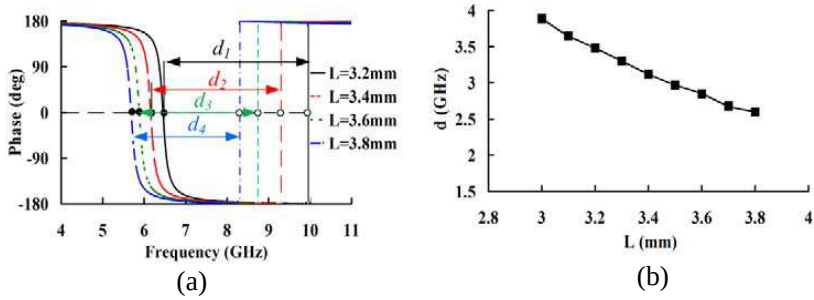

Figure 8. (a) Reflection phase curve with slot length $L = 3.2$ mm (black), 3.4 mm (red), 3.6 mm (green), 3.8 mm (blue). (b) Spectral distance (d) between AMC point and pole versus L. The other parameters are kept the same as those in Figure 2. As L increases, d decreases.

The reflection phase curve with different slot length is shown in Figure 8(a), and the spectral distance versus slot length is shown in Figure 8(b). Table 4 lists the related data. It is observed that when slot length is increased, the spectral distance decreases. For example, when the slot length is $L = 3.0\,\text{mm}$, the spectral distance is $d = 3.89\,\text{GHz}$. When the slot length is increased to $L = 3.8\,\text{mm}$, the spectral distance decreases to $d = 2.60\,\text{GHz}$. Similar to the effect of the substrate permittivity, both the AMC point and pole shift to lower frequency as the slot length increases, because when L is increased, the equivalent capacitance C_t increases.

3.5. Slot Width (W) Effect

Similar to the slot length (L), the width of the slots is also related to the equivalent capacitance C_t. In the following simulations, the slot width varies from 0.24 mm to 0.4 mm. The other parameters of the HSF-UC-EBG structure are kept the same as those in Figure 2. Figure 9(a) displays the reflection phase curve with different slot width and Figure 9(b) presents the spectral distance versus the slot width. The related data are listed in Table 5. It is observed that when the slot width (W) is changed, the spectral distance (d) remains almost the same. And the AMC point and pole slightly shift to lower frequency as W decreases. This is because when W decreases, the equivalent capacitance C_t increases according to Equations (5) and (6).

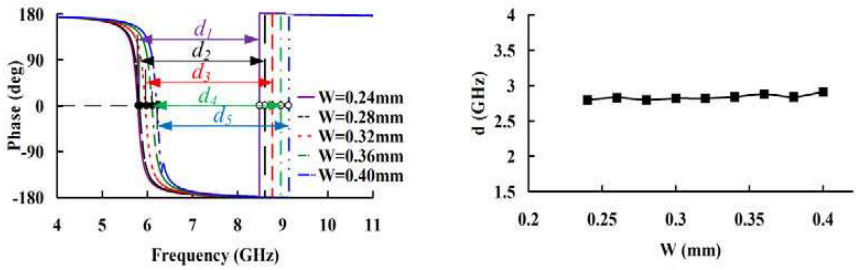

Figure 9. (a) Reflection phase curve with slot width $W = 0.24\,\text{mm}$ (violet), $W = 0.28\,\text{mm}$ (black), $0.32\,\text{mm}$ (red), $0.36\,\text{mm}$ (green), $0.40\,\text{mm}$ (blue). (b) Spectral distance (d) between AMC point and pole versus W. The other parameters are kept the same as those in Figure 2. When W is changed, d remains almost the same.

Table 5. Slot width effect.

W (mm)	AMC point (GHz)	Pole (GHz)	d (GHz)
0.24	5.68	8.48	2.80
0.26	5.75	8.58	2.83
0.28	5.83	8.63	2.80
0.30	5.90	8.72	2.82
0.32	5.95	8.77	2.82
0.34	6.03	8.87	2.84
0.36	6.10	8.98	2.88
0.38	6.18	9.02	2.84
0.40	6.21	9.12	2.91

4. TAILORING GUIDELINES AND DESIGNING EXAMPLE

4.1. Tailoring Guidelines

Based on the parametric study, the tailoring guidelines for reducing the spectral distance (d) between AMC point and pole, which is also the guidelines for designing UC-EBG structures with simultaneous AMC and EBG properties, can be summarize as following:

i) For a HSF-UC-EBG structure with fixed unit cell size, decreasing the substrate thickness (h), increasing the substrate permittivity (ε_r) and the slot length (L) are effective ways, while changing the slot width (W) makes little effect.

ii) The unit cell size can be scaled; increasing the scale factor (SF) of the unit cell size also makes great effect on reducing d.

4.2. Tailoring Example

Having obtained the design guidelines, one can tailor the AMC and EBG operation to coincide in the frequency domain very easily by following the reduction trend of the spectral distance (d). An example to design HSF-UC-EBG structure with simultaneous AMC and EBG operation is presented with detail steps in this section. The design steps follow the guidelines presented above, which can be seen from the three groups of parameters as shown in Table 6.

Compared to the first group of parameters, the substrate thickness (h) is decreased while the substrate permittivity (ε_r) is increased in the second group of parameters, and the other parameters are kept

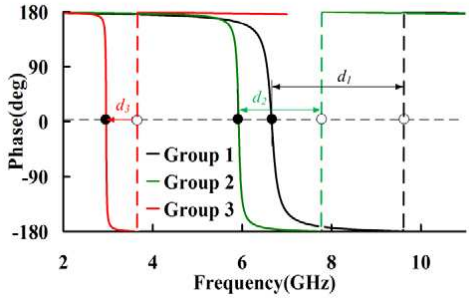

Figure 10. Reflection phase curve of the HSF-UC-EBG structure with parameters of Group 1 (black), Group 2 (green) and Group 3 (red).

Table 6. Three groups of parameters.

Group number	h (mm)	ε_r	SF	P (mm)	L (mm)	W (mm)
1	0.8	10.2	1	6	3.6	0.5
2	0.4	16	1	6	3.6	0.5
3	0.4	16	2	12	7.2	1.0

the same. The scale factor (SF) increases to 2 in the third group of parameters compared to the second group of parameters. Based on the guidelines, it is easy to predict that the spectral distance (d) between the AMC point and pole will be shortened as parameters change from Group 1 to Group 2, and further shortened when parameters change to Group 3. This trend is shown in Figure 10.

As demonstrate before, when the spectral distance between the AMC point and pole is shortened, the frequency region of AMC and EBG properties will be getting closer. And this trend is illustrated in Figures 11(a), (b) and (c). The AMC bandwidth is defined as the frequency rang within which the reflection phase is in the range of $+90^\circ$ to -90°. The dark and light gray region in Figure 11 represents the frequency region of AMC and EBG properties, respectively. It is observed that there is a long distance between the frequency region of the AMC and EBG properties in Figure 11(a); these two frequency regions become very close in Figure 11(b) as parameters changes from Group 1 to Group 2. Finally, the two frequency regions are partly overlapped when the HSF-UC-EBG structure with the parameters of Group 3, as shown in Figure 11(c). This overlapped area corresponds to simultaneous AMC and EBG properties in the frequency domain.

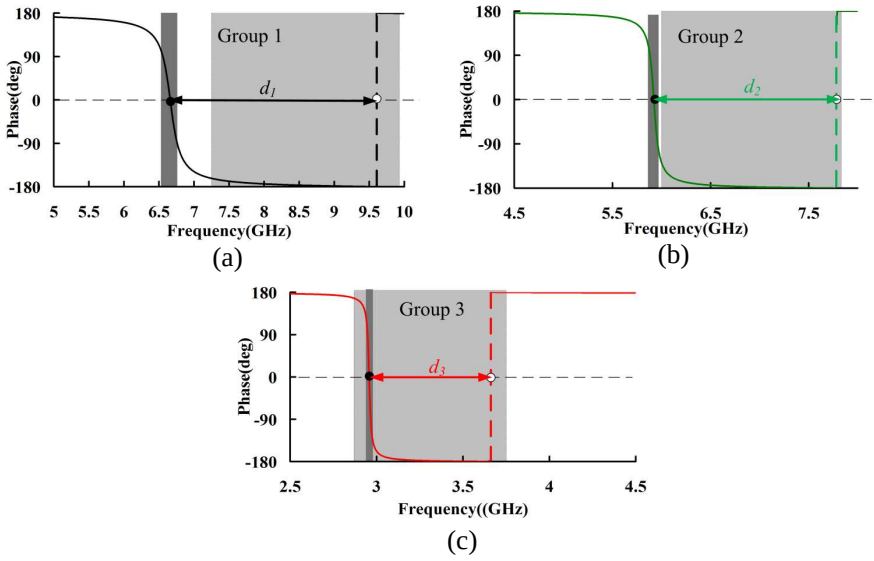

Figure 11. Spectral positions of the AMC (dark gray region) and EBG properties (light gray region) of the HSF-UC-EBG structure with parameters of (a) Group 1. (b) Group 2. (c) Group 3.

It is observed that the resonant frequency shifts to the lower frequency during the process, thus, the proposed method is useful when applied to the lower frequency region.

5. EXPERIMENTAL RESULTS

To validate our conclusions, the HSF-UC-EBG structure with simultaneous AMC and EBG properties was fabricated and measured. Figure 12 shows top view of the fabricated HSF-UC-EBG structure with parameters of $h = 0.4\,\text{mm}$, $\varepsilon_r = 16$, $P = 12\,\text{mm}$, $L = 7.8\,\text{mm}$, $W = 1.0\,\text{mm}$ (third group of parameters in Section 4). The measured S_{21} parameters in the Γ-X direction and Y-Γ direction, together with the reflection phase curve calculated in both HFSS and CST MWS are depicted in Figure 13. (Because the measurement of the reflection phase curve is restricted due to the limitations of our equipment, we use the CST MWS to validate the reflection phase curve data from HFSS).

As can be seen from Figure 13, the common SW bandgap (below $-20\,\text{dB}$) in the Γ-X direction and Y-Γ direction from the measurement is between 2.17–3.42 GHz (light gray region). The SW bandgap from

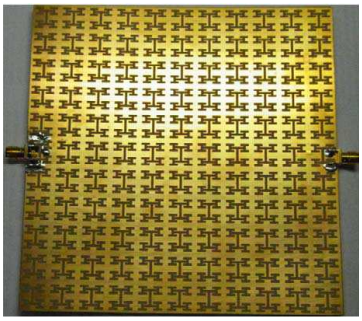

Figure 12. The top view of the fabricated HSF-UC-EBGs with parameters of $h = 0.4\,\text{mm}$, $\varepsilon_r = 16$, $P = 12\,\text{mm}$, $L = 7.8\,\text{mm}$, $W = 1.0\,\text{mm}$.

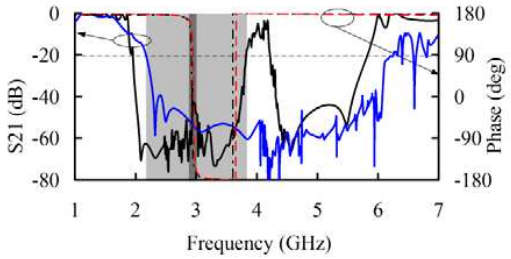

Figure 13. The measured S_{21} parameters in the Γ-X direction (black line) and Y-Γ direction (blue line), and reflection phase computed in HFSS (black dotted line) and in CST MWS (red dotted line) of the HSF-UC-EBG structure with parameters of $h = 0.4\,\text{mm}$, $\varepsilon_r = 16$, $P = 12\,\text{mm}$, $L = 7.8\,\text{mm}$, $W = 1.0\,\text{mm}$. Light gray region denote the common SW bandgap in Γ-X direction and Y-Γ direction, dark gray region denote the frequency region of the AMC property.

the dispersion diagram is 2.87–3.75 GHz (Figure 11(c)). Although, compared with the SW bandgap from the dispersion diagram, the measured SW bandgap moves to the lower frequency, which may caused by the manufacture errors, they are still in reasonable agreement in general. The reflection phase curve from CST MWS (red dotted line) is in good agreement with the results from HFSS (black dotted line). Simultaneous AMC and EBG properties (dark gray region) have been achieved as shown in Figure 13.

6. CONCLUSION

The relationship between the reflection phase curve and dispersion curve of a HSF-UC-EBG structure have been presented in this paper. It is demonstrated numerically and theoretically that the pole is located in the EBG location, and their frequency shift characteristics are the same. Based on this founding, we present a pole and AMC point matching method to design UC-EBG structure with simultaneous AMC and EBG properties, which is reducing the spectral distance (d) between the AMC point and pole. This is very valuable from the computational viewpoint since both the AMC point and pole belong to the reflection phase curve. Then a detail study on reducing d is presented. It is shown that decreasing the substrate thickness (h), increasing the substrate permittivity (ε_r), unit cell size and slot length (L) are effective ways to reduce d. Finally, in order to further demonstrate our finding, an example is presented to show the detail steps of designing HSF-UC-EBG structure with simultaneous AMC and EBG properties.

ACKNOWLEDGMENT

This research was supported in part by National 973 Program (No. 2012CB315705) and National 863 Program (Nos. 2011AA010306, 2011AA010303), P. R. China. Thanks for the great help.

REFERENCES

1. Coccioli, R., F. R. Yang, K. P. Ma, and T. Itoh, "Aperture-coupled patch antenna on UC-PBG substrate," *IEEE Transactions on Microwave Theory and Techniques*, Vol. 47, No. 11, 2123–2130, 1999.
2. Gnanagurunathan, G. and K. T. Selvan, "Gain enhancement of microstrip patch antenna by using complementary EBG geometries," *Journal of Electromagnetic Waves and Applications*, Vol. 26, Nos. 2–3, 329–341, 2012.
3. Pirhadi, A., M. Hakkak, and F. Keshmiri, "Bandwidth enhancement of the probe fed microstrip antenna using frequency selective surface as electromagnetic bandgap superstrate," *Progress In Electromagnetics Research*, Vol. 61, 215–230, 2006.
4. Yang, F., V. Demir, D. A. Elsherbeni, and A. Z. Elsherbeni, "Enhancement of dipole antennas characteristics using SEMI-EBG ground plane," *Journal of Electromagnetic Waves and Applications*, Vol. 20, No. 8, 993–1006, 2006.

5. Lamminen, A. E. I., A. R. Vimpari, and J. Säily, "UC-EBG on LTCC for 60-GHz frequency band antenna applications," *IEEE Transactions on Antennas and Propagation*, Vol. 57, No. 10, 2904–2912, 2009.
6. Nashaat, D., H. A. Elsadek, E. A. Abdallah, M. F. Iskander, and H. M. E. Hennawy. "Ultrawide bandwidth 2×2 microstrip patch array antenna using electromagnetic band-gap structure (EBG)," *IEEE Transactions on Antenna and Propagation*, Vol. 59, No. 5, 1528–1534, 2011.
7. Xie, H. H., Y. C. Jiao, L. N. Chen, and F. S. Zhang, "An effective analysis method for EBG reducing patch antenna coupling," *Progress In Electromagnetics Research Letters*, Vol. 21, 187–193, 2011.
8. Kim, S. H., T. T. Nguyen, and J. H. Jang, "Reflection characteristics of 1-D EBG ground plane and its application to a planar dipole antenna," *Progress In Electromagnetics Research*, Vol. 120, 51–66, 2011.
9. Gujral, M., J. L. W. Li, T. Yuan, and C. W. Qiu, "Bandwidth improvement of microstrip antenna array using dummy EBG pattern on feedline," *Progress In Electromagnetics Research*, Vol. 127, 79–92, 2012.
10. Huang, S. Y. and Y. H. Lee, "Compact U-shaped dual planar EBG microstrip low-pass filter," *IEEE Transactions on Microwave Theory and Techniques*, Vol. 53, No. 12, 3799–3805, 2005.
11. Chu, H., X. Q. Shi, and Y. X. Guo, "Utra-wideband bandpass filter with a notch band using EBG array etched ground," *Journal of Electromagnetic Waves and Applications*, Vol. 25, Nos. 2–3, 203–209, 2012.
12. Moghadasi, S. M., A. R. Attari, and M. M. Mirsalehi, "Compact and wideband 1-D mushroom-like EBG filters," *Progress In Electromagnetics Research*, Vol. 83, 323–333, 2008.
13. Shahparnia, S. and O. M. Ramahi. "Electromagnetic interference (EMI) reduction from printed circuit boards (PCB) using electromagnetic bandgap structures," *IEEE Transactions on Electromagnetic Compatibility*, Vol. 46, No. 4, 2004.
14. Ran, F., K. P. Ma, Y. Qin, and T. Itoh, "A uniplanar compact photonic-bandgap (UC-PBG) structure and its applications for microwave circuits," *IEEE Transactions on Microwave Theory and Techniques*, Vol. 47, No. 8, 1999.
15. Wu, T. L. and T. K. Wang, "Embedded power plane with ultra-wide stop-band for simultaneously switching noise on high-speed circuits," *Electronic Letter*, Vol. 42, No. 4. 213–241, 2006.

16. Hung, K. C., D. B. Lin, C. S. Chang, C. T. Wu, and I. T. Tang, "Novel fractal electromagnetic bandgap structures to suppress simultaneous switching noise in high speed circuits," *PIERS Proceedings*, Cambridge, USA, Jul. 2–6, 2008.
17. Ran, F., K. P. Ma, Y. Qin, and T. Itoh, "A novel TEM waveguide using uniplanar compact photonic-bandgap (UC-PBG) structure," *IEEE Transactions on Microwave Theory and Techniques*, Vol. 47, No. 11, 2092–2098, 1999.
18. Sievenpiper, D., L. Zhang, R. F. J. Broas, N. G. Alexopolous, and E. Yablonovitch, "High-impedance electromagnetic surfaces with a forbidden frequency band," *IEEE Transactions on Microwave Theory*, Vol. 47, No. 11. 2059–2074, 1999.
19. Goussetis, G., A. P. Feresidis, and J. C. Vardaxoglou, "Tailoring the AMC and EBG characteristics of periodic metallic arrays printed on trounded dielectric substrate," *IEEE Transactions on Antennas and Propagation*, Vol. 54. No. 1, 2006.
20. Kovács, P., Z. Raida, and M. M. Vázquez, "Parametric study of mushroom-like and planar periodic structures in terms of simultaneous AMC and EBG properties," *Radioengineering*, Vol. 17, No. 4, 19–24, 2008.
21. Christopoulos, N., G. Goussetis, A. P. Feresidis, and J. C. Vardaxoglou, "Metamaterials with multiband AMC And EBG properties," *Proceedings of European Microwave Week 2005*, Paris, France, Oct. 2005.
22. Hou, B., H. Xie, W. Wen, and P. Sheng, "Three-dimensional metallic fractals and their photonic crystal characteristics," *Physical Review B*, Vol. 77, No. 12, 125113(1–8), 2008.
23. Tchikaya, E. B., F. Khalil, F. A. Tahir, and H. Aubert. "Multi-scale approach for the electromagnetic simulation of finite size and thick frequency selective surfaces," *Progress In Electromagnetics Research M*, Vol. 17, 43–57, 2011.
24. Chiu, N., Y. C. Chang, H. C. Hsieh, and C. H. Chen, "Suppression of spurious emissions from a spiral inductor through the use of a frequency-selective surface," *IEEE Transactions on Electromagnetic Compatibility*, Vol. 52, No. 1, 56–63, 2010.
25. Cos, M. E., F. L. Heras, and M. Franco, "Design of planar artificial magnetic conductor ground plane using frequency-selective surfaces for frequencies below 1 GHz," *IEEE Antennas and Wireless Propagation Letters*, Vol. 8, 951–954, 2009.
26. Maci, S., M. Caiazzo, A. Cucini, and M. Casaletti, "A pole-zero matching method for EBG surfaces composed of dipole FSS printed on a grounded dielectric slab," *IEEE Transactions on*

Antenna and Propagation, Vol. 53, No. 1, 70–80, 2005.

27. Kim, J. H. and M. Swaminathan, "Modeling of irregular shaped power distribution planes using transmission matrix method," *IEEE Transactions on Advanced Packaging*, Vol. 54, No. 3, 334–346, 2001.
28. Kim, S. G., H. Kim, H. D. Kang, and J. G. Yook, "Modeling and analysis of a conventional and localized electromagnetic bandgap structures for suppression of simultaneous switching noise," *Microwave and Optical Technology Letters*, Vol. 54, No. 7, 1571–1577, 2012.